Supplement of

Influences of sources and weather dynamics on atmospheric deposition of Se species and other trace elements

Esther S. Breuninger[1,2], Julie Tolu[1,2], Iris Thurnherr[3], Franziska Aemisegger[3], Aryeh Feinberg[4], Sylvain Bouchet[1,2], Jeroen E. Sonke[5], Véronique Pont[6], Heini Wernli[3] and Lenny H.E. Winkel[1,2]

[1]Eawag, Swiss Federal Institute of Aquatic Science and Technology, Ueberlandstrasse 133, 8600 Dübendorf
[2]Institute of Biogeochemistry & Pollutant Dynamics, ETH Zurich, 8092 Zurich, Switzerland
[3]Institute for Atmospheric and Climate Science, ETH Zurich, 8092 Zurich, Switzerland
[4]Institute for Data, Systems, and Society, Massachusetts Institute of Technology, Cambridge, MA 02142, USA
[5]Géosciences Environnement Toulouse, CNRS/IRD/Université de Toulouse, 31400 Toulouse, France
[6]LAERO, Université de Toulouse, CNRS, IRD, UT3, 31400 Toulouse, France

Correspondence to: Esther S. Breuninger, Lenny H.E. Winkel

Table of Contents

S1: Additional information on ICP-MS/MS analysis

Table S1. ICP-MS/MS acquisition parameters used for each analysed elements in aerosol digests and water extracts, cloud water samples and precipitation samples.

Element	Collision/reaction cell gas and flow	MS Mode	*m/z*	Acquisition time (ms)
Li	H_2; 5 mL min^{-1}	MS/MS	7->7	50
Na	He; 5 mL min^{-1}	Single Quad	23	10
Mg	He; 5 mL min^{-1}	Single Quad	24	10
Al	He; 5 mL min^{-1}	Single Quad	27	10
Si	He; 5 mL min^{-1}	MS/MS	28->28	100
K	He; 5 mL min^{-1}	Single Quad	39	10
P	O_2; 30%	MS/MS	31->47	100
S	O_2; 30%	MS/MS	34->50	50
Ti	H_2; 5 mL min^{-1}	MS/MS	47->47	50
V	He; 5 mL min^{-1}	Single Quad	51	100
Cr	H_2; 5 mL min^{-1}	MS/MS	52->52	100
Mn	H_2; 5 mL min^{-1}	MS/MS	55->55	50
Fe	He; 5 mL min^{-1}	Single Quad	56	50
Co	H_2; 5 mL min^{-1}	MS/MS	59->59	100
Ni	He; 5 mL min^{-1}	Single Quad	60	50
Cu	He; 5 mL min^{-1}	Single Quad	63	100
Zn	H_2; 5 mL min^{-1}	MS/MS	66->66	100
As	O_2; 30%	MS/MS	75->91	300
Se	H_2; 5 mL min^{-1}	MS/MS	78->78 80->80	300
Br	O_2; 30%	MS/MS	81->97	100
Rb	H_2; 5 mL min^{-1}	MS/MS	85->85	50
Sr	He; 5 mL min^{-1}	Single Quad	88	50
Nb	H_2; 5 mL min^{-1}	MS/MS	93->93	100
Mo	H_2; 5 mL min^{-1}	MS/MS	98->98	100
Ag	H_2; 5 mL min^{-1}	MS/MS	107->107	100
Cd	H_2; 5 mL min^{-1}	MS/MS	111->111	100
I	O_2; 30%	MS/MS	127->127	100
Cs	H_2; 5 mL min^{-1}	MS/MS	133->133	100
Ba	H_2; 5 mL min^{-1}	MS/MS	135->135	50
Pb	H_2; 5 mL min^{-1}	MS/MS	208->208	100

Table S2. Elements analysed as internal standards during total element analysis along with information on used ICP-MS/MS acquisition parameters.

Element	Collision/reaction cell gas and flow	MS Mode	*m/z*	Acquisition time (ms)
Sc	H_2; 5 mL min^{-1}	MS/MS	45->45	50
Sc	O_2; 30%	MS/MS	45->61	50
Sc	He; 5 mL min^{-1}	Single Quad	45	50
Y	H_2; 5 mL min^{-1}	MS/MS	89->89	50
Y	O_2; 30%	MS/MS	89->105	50
Y	He; 5 mL min^{-1}	Single Quad	89	50
In	H_2; 5 mL min^{-1}	MS/MS	115->115 118->118	50
In	O_2; 30%	MS/MS	115->131	50
In	He; 5 mL min^{-1}	Single Quad	115 118	50
Lu	H_2; 5 mL min^{-1}	MS/MS	175->175	50
Lu	O_2; 30%	MS/MS	175->191	50
Lu	He; 5 mL min^{-1}	Single Quad	175	50

Table S3. Recoveries (%) and error (%) obtained for measured elements in two certified reference materials (CRMs) which were analysed with the atmospheric samples. The CRMs were analysed after their dilution (d10 or d100) in the corresponding sample matrix, i.e., 1% HNO_3 for precipitation, cloud water and aerosol water extracts, and 16-26 % HNO_3 for aerosol digests. Analysed replicates for each CRM are indicated by N.

	Precipitation & Cloud water (1% HNO_3)						**Aerosol Extract** (16-26% HNO_3)					
	Certified element concentration ($\mu g\ L^{-1}$)	**Recoveries[a]** (%) av[c] sd[d]	**Error[b]** (%)	**Used Dilution**	**N**	**Recoveries[a]** (%) av[c] sd[d]	**Error[b]** (%)	**Used Dilution d**	**N**
CRM NIST 1643f, Trace Elements in Water									
Li	16.6 ± 0.4	**103** ± 9	**3**	d10, d100	4	**99.5** ± 4	**-0.5**	d10, d100	6
Na	18830 ± 250	**102** ± 2	**2**	d10, d100	4	**98** ± 2	**-2**	d10, d100	12
Mg	7454 ± 60	**103** ± 2	**3**	d10, d100	4	**102.7** ± 1.1	**2.7**	d10, d100	12
Al	133.8 ± 1.2	±			4	**105** ± 3	**5**	d10, d100	12
K	1933 ± 9	**100.4** ± 6.7	**0.4**	d10	4	**98.5** ± 0.7	**-1.5**	d10, d100	12
V	36.1 ± 0.3	**105** ± 0	**5**	d10	4	**103** ± 2	**3**	d10, d100	6
Cr	18.5 ± 0.1	**101** ± 8	**1**	d10, d100	4	**105** ± 3	**5**	d10, d100	6
Mn	37.1 ± 0.6	**103** ± 4	**3**	d10, d100	4	**98.7** ± 2.3	**-1.3**	d10, d100	6
Fe	93.4 ± 0.8	**105** ± 3	**5**	d10	4	**101.8** ± 0.5	**1.8**	d10, d100	12
Co	25.3 ± 0.2	**98** ± 4	**-2**	d10, d100	4	**103.0** ± 0.1	**3.0**	d10, d100	6
Ni	59.8 ± 1.4	**99.6** ± 3.0	**-0.4**	d10, d100	4	**101.9** ± 0.4	**1.9**	d10, d100	6
Cu	21.7 ± 0.7	**102** ± 7	**2**	d10, d100	4	**102.3** ± 1.6	**2.3**	d10, d100	6
Zn	74.4 ± 1.7	**102** ± 4	**2**	d10	4	**105** ± 3	**5**	d10	6
As	57.4 ± 0.4	**99** ± 0.7	**-1**	d10, d100	4	**103.7** ± 0.7	**3.7**	d10, d100	6
^{78}Se	11.7 ± 0.1	**99** ± 1	**-1**	d10, d100	4	**102.9** ± 0.5	**2.9**	d10, d100	6
^{80}Se	11.7 ± 0.1	**99.2** ± 0.4	**-0.8**	d10, d100	4	**101.2** ± 0.1	**1.2**	d10, d100	6
Rb	12.6 ± 0.1	**97** ± 7	**-3**	d10	4	**105.5** ± 1.0	**5.5**	d10, d100	6
Sr	314 ± 19	**101** ± 5	**1**	d10, d100	4	**103.2** ± 1.4	**3.2**	d10, d100	6
Mo	115.3 ± 1.7	**99** ± 5	**-1**	d10, d100	4	**103.4** ± 0.4	**3.4**	d10, d100	6
Ag	1.0 ± 0.0	**97** ± 7	**-3**	d10	4	**107** ± 4	**7**	d10	6
Cd	5.9 ± 0.1	**102** ± 4	**2**	d10, d100	4	**102** ± 3	**2**	d10, d100	6
Ba	518.2 ± 7	**102** ± 2	**2**	d10, d100	4	**102.2** ± 0.2	**2.2**	d10, d100	6
Pb	18.5 ± 0.1	**99.7** ± 1.7	**-0.3**	d10	4	**103.1** ± 1.5	**3.1**	d10, d100	6
CRM TMDA 51.2, Trace Elements in Surface Water (Lake Ontario)									
Al	96 ± 19					**99.2** ± 7.8	**-0.8**	d10	6
V	48 ± 8	**102** ± 2	**2**	d10, d100	4	**102.7** ± 0.5	**2.7**	d10, d100	6
Cr	63 ± 7	**97** ± 5	**-3**	d10, d100	4	**103.8** ± 1.3	**3.8**	d10, d100	6
Mn	82 ± 10	**98** ± 2	**-2**	d10, d100	4	**102.0** ± 1.0	**2.0**	d10, d100	6
Fe	111 ± 26	**108** ± 6	**8**	d10	4	**103** ± 3	**3**		6
Co	72 ± 6	**94** ± 8	**-6**	d10, d100	4	**104.8** ± 1.0	**4.8**	d10, d100	6
Ni	67 ± 7	**97.7** ± 0.9	**-2.3**	d10, d100	4	**104.9** ± 0.3	**4.9**	d10, d100	6
Cu	91 ± 10	**99** ± 3	**-1**	d10, d100	4	**104.4** ± 1.2	**4.4**	d10, d100	6
Zn	106 ± 15	**102** ± 3	**2**	d10	4	**105.6** ± 0.4	**5.6**	d10, d100	6
As	15 ± 3	**96.0** ± 1.2	**-4**	d10, d100	4	**103.1** ± 0.9	**3.1**	d10, d100	6
^{78}Se	12 ± 3	**96.7** ± 0.3	**-3.3**	d10, d100	4	**97.6** ± 0.3	**-2.4**	d10, d100	6
^{80}Se	12 ± 3	**96.0** ± 1.2	**-4**	d10, d100	4	**98.4** ± 2.0	**-2**	d10, d100	6
Sr	121 ± 12	**96** ± 4	**-4**	d10	4	**101.7** ± 0.4	**1.7**	d10, d100	6
Mo	59 ± 6	**97** ± 5	**-3**	d10, d100	4	**106.3** ± 1.0	**6.3**	d10, d100	6
Cd	25 ± 3	**99.2** ± 1.0	**-0.8**	d10, d100	4	**103** ± 2	**3**	d10, d100	6
Ba	73 ± 6	**99** ± 3	**-1**	d10, d100	4	**104.3** ± 0.8	**4.3**	d10, d100	6
Pb	73 ± 11	**99** ± 4	**-1**	d10, d100	4	**102.0** ± 0.5	**2.0**	d10, d100	6

[a]Recoveries were calculated as follows: (element concentration measured)/(element concentration certified) x 100; [b]Errors were calculated as follows: [(element concentration measured)-(element concentration certified)] / (element concentration certified) x100; [c]av.: average; [d]sd: standard deviation

S2: Extraction and pre-concentration of Se species in atmospheric samples

S2.1 Extraction of Se species from aerosol filter samples

We developed a method for extraction of selenium (Se) species from aerosol samples. For a better comparison to sampled precipitation, our focus was on the water-soluble fraction of aerosols. The extraction of Se species from aerosol samples was done as follows: 11.404 cm^2 of aerosol filter (corresponding to 7197±1816 m^3 of sampled air) was placed in a polyporopylene tube with 15 mL of ultrapure water, the mixture was then sonicated twice for 20 min at 20°C, and finally filtered after extraction (0.22 µm, Nylon). The sonication was done twice for 20 min instead of full 40 min to avoid increases of the sample temperature, which is known to potentially cause species transformation (Gómez-Ariza et al., 1999).

Stability of Se^{IV}, Se^{VI}, SeMet and $SeCys_2$ was determined by measuring recoveries of initial species concentration of 200 $ng \cdot L^{-1}$ after sonication by HPLC-ICP-MS/MS (specification on methods in S3). Se^{IV}, Se^{VI} and $SeCys_2$ showed high recoveries, i.e., 101±2%, 101±2% and 96±0.4%, respectively. However, recoveries of SeMet were lower, i.e., of 65±3%, indicating that sonication caused a partial transformation of SeMet species. Prior to lyophilisation of the aerosol extracts, ammonium citrate was added (to match mobile phase concentration of LC method after lyophilisation).

Overall extraction efficiencies of the water-soluble fraction of aerosols were determined by comparison between total Se concentrations in the water extract and the total acid digestion by ICP-MS/MS (method specification in S1 for total analysis and S3 for speciation analysis). Extraction efficiencies in the water extracts of the 2015-2020 aerosol time series (n=70) were 85±18% for Se and 100±10% for sulfur (S) species.

S2.2 Pre-concentration of Se species in atmospheric samples

We developed a method to pre-concentrate atmospheric samples based on lyophilisation using inorganic Se species (i.e., Se^{IV} and Se^{VI}) that have been previously identified in rainwater (Suess et al., 2019; Roulier et al., 2021) as well as potentially present organic species for which standards are commercially available, i.e., $SeCys_2$ and SeMet. Different parameters were tested including the effects of ionic strength, sampling containers, as well as lyophilisation to complete dryness versus lyophilisation to a residual volume. For each test, Se species recovery and stability were assessed.

The first experiments consisted of lyophilisation to complete dryness of:

- Solutions of individual Se species (200 $ng \cdot L^{-1}$) in ultrapure water
- Solutions of individual Se species (200 $ng \cdot L^{-1}$) in a 2 $mmol \cdot L^{-1}$ ammonium citrate solution to match mobile phase concentration of LC method (described in S3) after lyophilisation
- Three different rainwater samples collected at Pic du Midi Observatory (previously stored at 4°C) and spiked with individual Se species (50 $ng \cdot L^{-1}$).

Recoveries were determined by comparison between the initial concentration of spiked Se species and the final recovered Se species (i.e., after lyophilisation) determined using HPLC-ICP-MS/MS. Se species recoveries are shown in Fig. S1 and demonstrate that lyophilisation to complete dryness leads to transformation and losses of Se species in all different tested matrices. The lowest recoveries were obtained for Se species in ultrapure water (Se^{IV}: 64±8%, Se^{VI}: 78±0.3%, SeMet: 12±0.2%, $SeCys_2$: 8±1%) followed by Se species in rainwater (Se^{IV}: 85±16%, Se^{VI}: 106±12%, SeMet: 58±10%, $SeCys_2$: 22±8%) and finally those for Se species in 2 $mmol \cdot L^{-1}$ ammonium citrate (Se^{IV}: 90±1%, Se^{VI}: 100±0.3%, SeMet: 80±0.3%, $SeCys_2$: 103±1%). We particularly observed losses of the organic Se species SeMet and $SeCys_2$ in ultrapure water and rainwater (Fig. S1). Lyophilisation of tested organic Se species in relatively low ionic strength solutions might lead to transformation to other organic Se species that are not retained by anion exchange. Overall, the results suggest a significant influence of ionic strength on Se species recoveries, with higher recoveries of Se species during lyophilisation at increased ionic strength.

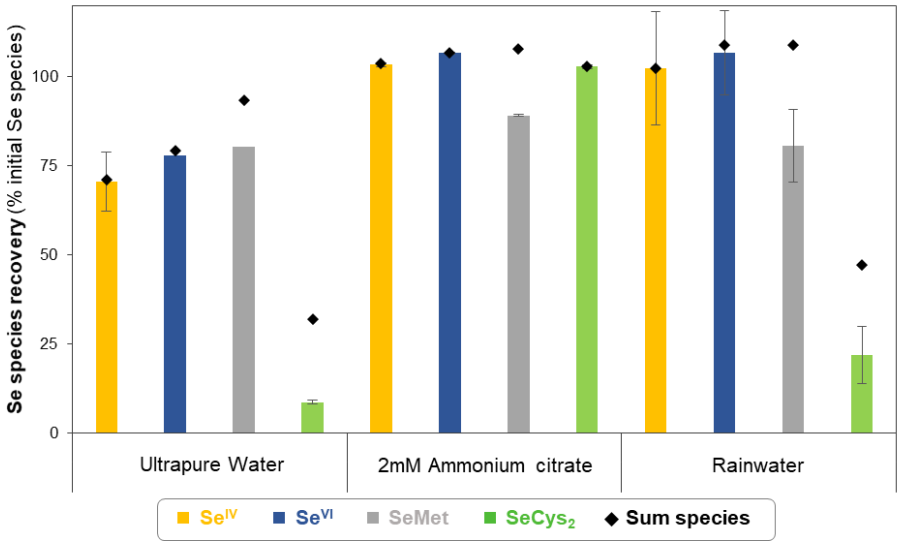

Fig. S1. Recoveries of individual Se species during lyophilisation to complete dryness in different matrices. Tested matrices included ultrapure water, a 2 mmol·L^{-1} ammonium citrate solution (eluent of LC-method) and three different rainwater samples collected at Pic du Midi Observatory. Recoveries of single Se species are displayed as bar plots (% of initial Se species concentrations). The sum of concentrations of all recovered Se species are displayed as diamonds for each tested solution. The error bars represent the standard deviation values resulting from quantification by LC-ICP-MS/MS in duplicate.

The following tests aimed at investigating the effect of different types of containers used for the lyophilisation on the Se species recoveries. The tested containers for lyophilisation included:

- Greiner polypropylene centrifuge tubes "PP-Greiner" (Huber)
- metal free-centrifuge tubes (VWR)
- Perfluoralkoxy (PFA) tubes (AHF, Analysentechnik AG)

Compared to when using lyophilisation of sample to complete dryness, all Se species were entirely recovered with lyophilisation to a residual volume of <1.5 mL, and this was true for all tested containers (Fig. S2). The Greiner centrifugation tubes were thus chosen for collection of field samples and their processing, i.e., lyophilisation.

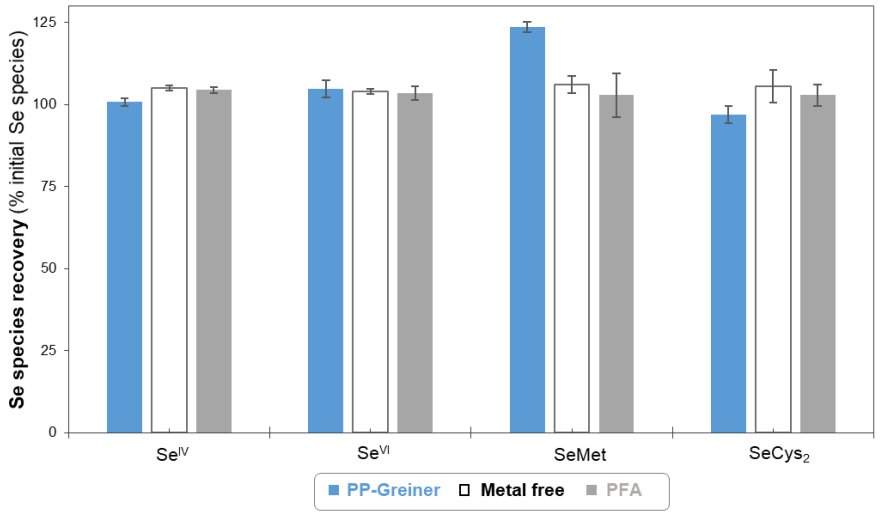

Fig. S2. Recoveries Se species during lyophilisation to a residual volume in different tested containers. Lyophilisation was done with addition of 2 mmol·L^{-1} ammonium citrate solution (eluent of LC-method). Tested lyophilisation containers included polypropylene (PP) Greiner centrifuge tubes, metal free-centrifuge tubes and perfluoralkoxy (PFA) tubes. Recoveries of Se species are displayed as bar plots (% of initial Se species concentrations). The error bars represent the standard deviation values resulting from three independent replicates and subsequent quantification by LC-ICP-MS/MS in duplicate.

In addition to above tested parameters, the ratio of initial to residual volume should be considered. Our optimized pre-concentration method involves the lyophilisation of frozen precipitation samples from an initial volume of

12 mL (for precipitation) or 9 mL (for water extract of aerosol filter) to a residual volume of 1.5 mL (pre-concentration factor of 8 or 6, respectively). These pre-concentration factors were found to be sufficient to determine Se speciation in atmospheric samples collected at remote sites with limited available samples volumes. Different ratios of initial to residual volume, especially much higher initial samples volumes compared to low residual volumes (1.5 mL) will likely lead to poorer Se species recoveries and would need to be tested in future studies.

S3: LC-ICP-MS/MS method optimization and detailed procedures

The optimization of the LC-ICP-MS/MS method to determine Se speciation in atmospheric samples was aimed at optimizing a method previously used for Se speciation in soil extracts and water samples (e.g., Tolu et al. (2011); Darrouzès et al. (2008)) in order to achieve:

1) lower solvent and sample consumption
2) lower running time (i.e. analysis time per sample)
3) lower detection limits for different Se species (i.e., Se^{IV}, Se^{VI}, SeMet, and $SeCys_2$)

In the previous method by Tolu et al. (2011), an anion exchanges chromatography column (Hamilton PRP-X100, 250×4.1 mm, 10 μm) was used with an isocratic elution of ammonium citrate (5 mM, 2% MeOH, pH 5.2) delivered at 1 $mL \cdot min^{-1}$, injection volumes of 100-400 μL and a total measurement time of 15 min.
Here, we used the same column type, however with smaller inner column diameter (i.e., 2.1 mm vs 4.1 mm) to reduce solvent and sample consumption (reduction of mobile phase flow rate and sample injection volume), smaller column length (i.e., 150 vs 250 mm) to reduce measurement time, as well as smaller particle size (i.e., 5 vs 10 μm) to increase retention of Se species. Furthermore, we optimized the gradient elution (Table S4 and Fig. S3) of tested Se species to reduce measurement time and to improve peak shapes and thus lower detection limits of Se species.

Table S4. Gradient of the LC-ICP-MS/MS method used for the speciation analysis of Se. Eluents were as follows: A = ultrapure water, and B= 20 $mmol \cdot L^{-1}$ ammonium citrate.

Time (min)	**Ammonium Citrate concentration** ($mmol \cdot L^{-1}$)	**Percentage of eluent A** (%)	**Percentage of eluent B** (%)
0.9	5.2	74	26
1.5	13	35	65
1.8	13	35	65
1.95	5.2	74	26
5.25	5.2	74	26

Fig. S3 shows the LC-ICP-MS/MS chromatogram obtained with a mixed standard solution of 1 $\mu g \cdot L^{-1}$ using our optimized separation (orange chromatogram) and using the method of Tolu et al. (blue chromatogram). In comparison to the previous method by Tolu et al. (2011), peak shape (both height and width) was greatly improved, and analysis time (5.4 min), consumption of solvent 0.5 $mL \cdot min^{-1}$ and injection volume (20 μL) was significantly reduced.

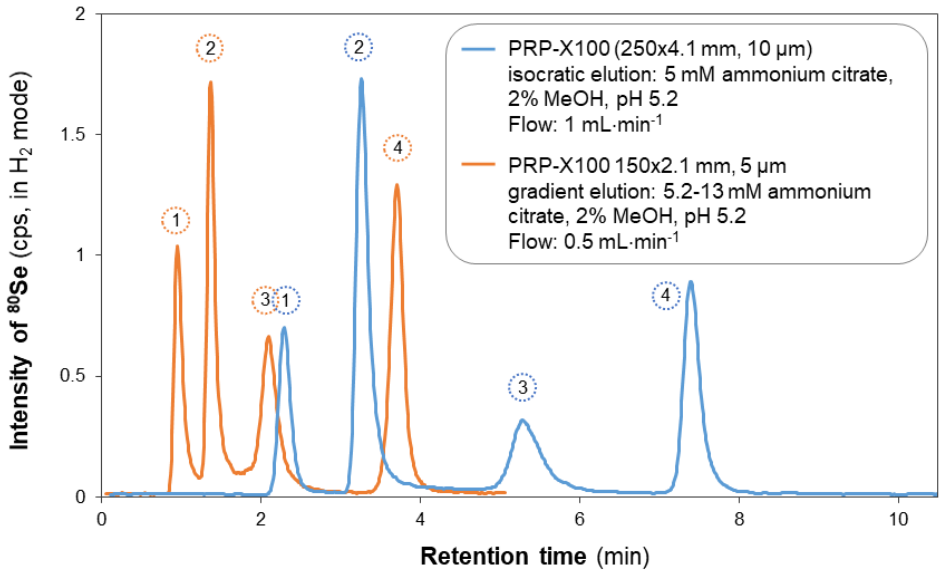

Fig. S3. Comparison of Se intensity chromatogram obtained for a multi-Se species standard using the initial LC-ICP-MS method described by Tolu et al. (blue line) and with the optimized LC-ICP-MS/MS method (orange line). The multi-Se species standard contained 1 µg(Se)·L^{-1} of (1) $SeCys_2$, (2) Se^{IV}, (3) SeMet and (4) Se^{VI}. The initial LC-ICP-MS method described by Tolu et al. (blue line) involves a PRP-X100 column (250x4.1 mm, 10 µm), an isocratic elution using a mobile phase consisting of 5 mmol·L^{-1} ammonium citrate and 2% MeOH at pH 5.2, a flow of 1 mL·min^{-1} and an injection volume of 100 µL. Our optimized LC-ICP-MS/MS method (orange line) involves a PRP-X100 column (150x2.1 mm, 5 µm), a gradient elution from 5.2 to 13 mmol·L^{-1} ammonium citrate with 2% MeOH, at pH 5.2, a flow of 0.5 mL·min^{-1} and an injection volume of 20 µL. Shown chromatograms were obtained without adding tetramethylammonium hydroxide (TMAH) post-column.

Finally, 14% v/v tetramethylammonium hydroxide (TMAH) was added to the internal standard solution, which was continuously supplied post-column through a T-piece by using the peristaltic pump of the ICP-MS/MS, to further increase the sensitivity of Se analyses via the well-known carbon enhancement effect (Larsen and Stürup, 1994). The addition of TMAH resulted in an increase of sensitivity of approximately 3.5. With this set-up and considering the pre-concentration step, detection limits of 1-2 ng·L^{-1} were reached.

Table S5. LC-ICP-MS/MS operating conditions for speciation analysis of Se.

LC system	**Agilent 1260 Infinity II Bio-Inert high performance LC System**
Column	Hamilton PRPX-100, 150x2.1mm, 5 µm
Injection Volume	20 µL
Mobile Phase	Ammonium Citrate (optimized) - 2 % MeOH, pH 5.2
Flow Rate	0.5 mL min^{-1}
ICP-MS/MS system	**8900 Agilent ICP-MS/MS**
Configuration	Quartz torch (2.5 mm id), Ni cones, x-lenses
RF power	1550 W
Spray Chamber	Scott type, + 2°C
Nebulizer Gas	1.09 L min^{-1}
Make up Gas	0.12 L min^{-1}
Cell Gas	5 ml min^{-1} of H_2
Acquisition time	100 ms for ^{74}Se, ^{76}Se, ^{77}Se, ^{78}Se, ^{80}Se, ^{82}Se, 50 ms for Br and 10 ms for Y

Table S6. LC-ICP-MS/MS operating conditions for speciation analysis of sulfur (S) as published previously by Müller et al. (2019).

LC system	**Agilent 1260 Infinity I Bio-Inert high performance LC System**
Column	Thermofisher Hypercarb, 100x4.6 mm, 5 µm
Injection Volume	50 µL
Mobile Phase	Formic acid 24-240 mmol L^{-1} - 1 % MeOH, pH 2.1
Flow Rate	1 mL min^{-1}
ICP-MS/MS system	**8800 Agilent ICP-MS/MS**
Configuration	Quartz torch (2.5 mm id), Ni cones, x-lenses
RF power	1550 W
Spray Chamber	Scott type, + 2°C
Nebulizer Gas	1.10 L min^{-1}
Make up Gas	0.12 L min^{-1}
Cell Gas	30% of O_2 with 2 ml min^{-1} of H_2
Acquisition time	50 ms for ^{32}S and 20 ms for Sc, Y

S4: Identification of organic compounds by Py-GC-MS

The analysis of organic compounds in aerosols was performed on a FrontierLab pyrolyzer equipped with a FrontierLab AS-1020E autosampler and connected to a Thermoscientific Trace 1310 GC coupled to a Thermoscientific ISQ 7000 MS. The operating conditions and subsequent data processing method were followed as described in Tolu et al. (2015). Briefly, the pyrolysis was performed at 450°C and the temperatures of the Py-GC interface, GC injector and GC-MS interface were set to 320°C and 300°C, respectively. The injector was operated with He as the carrier gas (at 1.2 $mL \cdot min^{-1}$) and a split ratio of 16:1. After one minute the gas-saver mode was used with a flow rate of 10 $mL \cdot min^{-1}$ to vent away the pyrolysate bleed of the sample remaining in the pyrolyzer oven. The pyrolysate was separated on a DB-5MS capillary column (30 m x 0.25 mm, 0.25 mm film thickness; J&W, Agilent Technologies AB, Sweden) and the GC temperature program increased from 40°C with a rate of 10 $C \cdot min^{-1}$ to 320°C, which was held for 5 min. The mass spectrometer with a quadrupole type analyser was operated at unit mass resolution and scanned the mass range from *m/z* 45 to 650 at 3.1 $scan \cdot s^{-1}$. 70 eV electron bombardment was used for ionization. Peak integration was done using a data processing pipeline under the "R" computational environment. Peak identification was then made using the software "NIST MS Search 2" containing the library "NIST/EPA/NIH 2011" and additional spectra from published studies (Tolu et al., 2015). In total, 105 Py-compounds from 11 classes (e.g. carbohydrates, N compounds, (poly)aromatics) were identified in warm season aerosol samples, respectively (Table S7), along with information on their molecular mass and chemical formula and references for the theoretical mass spectra. For each compound, relative abundance was calculated by setting the total identified peak area for each sample to 100%. The individual Py-products were grouped based on similarities in the molecular structure and origin, which were used for statistical analysis (see defined compound groups in Table S7).

Table S7. List of organic compounds identified by Py-GC-MS in the aerosols from the 2015-2020 time series together with information on their formula, molecular mass (M), specific mass fragments, references for the mass spectra and the compound sub-groupings used for the statistical analyses.

Name	Formula	M	Specific mass fragments	Ref	Compound sub-groups
Carbohydrates					
4,4-Dimethyl-2-cyclopenten-1-one	C7H10O	110	41+67+**95**+110	NIST	(Cyclo)pentenone/-dione
4-Cyclopentene-1,3-dione	C5H4O2	96	26+42+54+68+**96**	NIST	
3-Furaldehyde	C5H4O2	96	39+67+**95**+96	NIST	(alkyl)furans/ -furanones
2(3H)-Furanone, 5-methyl-	C5H6O2	98	27+43+**55**+98	NIST	
2(5H)-Furanone	C4H4O2	84	39+55+84	NIST	
2(5H)-Furanone, 5,5-dimethyl-	C6H8O2	112	43+96+**97**	NIST	
(3H)-Furanone, dihydro-5-methyl-	C5H8O2	100	56+85+100	NIST	
2-Furaldehyde, 5-methyl-	C6H6O2	110	27+53+**110**	NIST	
4-Methyl-5H-furan-2-one	C5H6O2	98	39+40+41+**69**+98	NIST	
2(5H)-Furanone, 3,5,5-trimethyl-	C7H10O2	126	83+111	NIST	
2(3H)-Benzofuranone	C8H6O2	134	**78**+106+134	NIST	
1,4:3,6-Dianhydro-α-d-glucopyranose	C6H8O4	144	29+41+57+**69**	NIST	Levoglucosan or fresh polyaccharides
β-D-Glucopyranose, 1,6-anhydro-	C6H10O5	162	29+57+**60**+73	NIST	
Carboxylic acids					
2-Propenoic acid	C3H4O2	72	26+27+45+55+**72**	NIST	Alkanoic acids C3-C12
2-Pentenoic acid, 2-methyl-, (E)-	C6H10O2	114	27+39+41+**69**+114	NIST	
Pinonic acid	C10H16O3	184	69+83+98+114+125	NIST	
Dodecanoic acid	C12H24O2	200	41+43+55+57+60+**73**	NIST	
Tetradecanoic acid	C14H28O2	228	41+43+55+57+60+**73**+129+228	NIST	Alkanoic acids C14-C18
Pentadecanoic acid	C15H30O2	242	41+43+55+57+60+**73**+129+242	NIST	
Hexadecanoic acid	C16H32O2	256	41+**43**+55+57+60+73+129+256	NIST	
Octadecenoic acid	C18H34O2	282	55+69+83+97+123+264+282	NIST	
Octadecanoic acid	C18H36O2	284	41+**43**+55+57+60+73+129+284	NIST	
Alkanoic acid methyl ester			74+87+255+298	NIST	Alkanoic acids >C18
Alkanoic acid C22:0	C22H44O2	332	41+**43**+55+57+60+73+129+332	NIST	
N-compounds					
Pyrrole+pyridine	(C4H5N)+(C5H5N)	(83)+(79)	(50+51+52+**79) + (67)**	NIST	(alkyl)pyrroles/ -pyridines
Pyrrole	C4H5N	67	37+38+**39**+40+**41**+**67**	NIST	
1H-Pyrrole, 2-methyl-	C5H7N	81	**80**+81	NIST	
Pyridine, 3-methyl-	C6H7N	93	39+65+66+92+**93**	NIST	
Pyridine, 2,4,6-trimethyl-	C8H11N	121	79+106+**121**	NIST	
Pyrazole-5-carboxylic acid	C4H4N2O2	112	66+94+95+112	NIST	
1H-Pyrrole-2,5-dione, 1-methyl-	C5H5NO2	111	26+54+83+83+**111**	NIST	
2,5-Pyrrolidinedione (succinimide)	C4H5NO2	99	59+99	NIST	
1H-Pyrazole, 1,3,5-trimethyl-	C6H10N2	110	95+**110**	NIST	
Acetamide	C2H5NO	59	42+43+**44+59**	NIST	Alkylamides

Alkylamide1	unknown		**59**+72	NIST	
Alkylamide2	unknown		**59**+72	NIST	
Alkylamide3	unknown		**59**+72	NIST	
Docosenamide	C22H43NO	337	**59+72**+240+277+294+320+337	NIST	
Diketopiperazine (DKP) Pro-Pro	C10H14N2O2	194	70+96+138+166+ **194**	[1, 2]	Proteins
Diketopiperazine (DKP) Pro-Lys-NH3	unknown	208	70, 125, 154, 166, **208**	[1, 2]	
Octadecanenitrile	C18H35N	265	**57**+70+97+110+ 124	NIST	
alkanenitrile1	unknown	x	**57**+70+97+110+ 124	NIST	
alkanenitrile2	unknown	x	**57**+70+97+110+ 124	NIST	Alkylnitriles
alkanenitrile3	unknown	x	**57**+70+97+110+ 124	NIST	
alkanenitrile4	unknown	x	**57**+70+97+110+ 124	NIST	
***n*-alkenes**					
n-C13:1	C13H26	182	56+69+…+182	NIST	C13 (odd n°)
n-C14:1	C14H28	196	56+69+…+196	NIST	
n-C16:1	C16H32	224	56+69+…+224	NIST	C14 to C20 (even n°)
n-C18:1	C18H36	252	56+69+…+252	NIST	
n-C20:1	C20H40	280	56+69+…+280	NIST	
n-C15:1	C15H30	210	56+69+…+210	NIST	
n-C17:1	C17H34	238	56+69+…+238	NIST	C15 to C19 (odd n°)
n-C19:1	C19H38	266	56+69+…+266	NIST	
n-C21:1	C21H42	294	56+69+…+294	NIST	
n-C23:1	C23H46	322	56+69+…+322	NIST	
n-C25:1	C25H50	350	56+69+…+350	NIST	C21 C33 (odd n°)
n-C29:1	C29H58	406	56+69+…+406	NIST	
n-C31:1	C31H62	434	56+69+…+434	NIST	
n-C33:1	C33H66	462	56+69+…+462	NIST	
n-C22:1	C22H44	308	56+69+…+308	NIST	
n-C24:1	C24H48	336	56+69+…+336	NIST	C22 to C26 (even n°)
n-C26:1	C26H52	364	56+69+…+364	NIST	
***n*-alkanes**					
n-C14:0	C14H30	198	57+71+85+…+198	NIST	
n-C18:0	C18H38	254	57+71+85+…+254	NIST	C14 to C20 (even n°)
n-C20:0	C20H42	282	57+71+85+…+282	NIST	
n-C15:0	C15H32	212	57+71+85+…+212	NIST	
n-C17:0	C17H36	240	57+71+85+…+240	NIST	C15 to C19 (odd n°)
n-C19:0	C19H40	268	57+71+85+…+268	NIST	
n-C21:0	C21H44	296	57+71+85+…+296	NIST	
n-C23:0	C23H48	324	57+71+85+…+324	NIST	
n-C25:0	C25H52	352	57+71+85+…+352	NIST	
n-C27:0	C27H56	380	57+71+85+…+380	NIST	C21 to C37 (odd n°)
n-C29:0	C29H60	408	57+71+85+…+408	NIST	
n-C31:0	C31H64	436	57+71+85+…+436	NIST	
n-C37:0	C37H76	521	57+71+85+…+521	NIST	
n-C22:0	C22H46	311	57+71+85+…+310	NIST	C22 to C38 (even n°)

n-C24:0	C24H50	338	57+71+85+…+338	NIST	
n-C32:0	C32H66	450	57+71+85+…+450	NIST	
n-C34:0	C34H70	480	57+71+85+…+480	NIST	
n-C36:0	C36H74	506	57+71+85+…+506	NIST	
n-C38:0	C38H78	535	57+71+85+…+535	NIST	
Alkanones					
2-Pentadecanone	C15H30O	226	43+**58**+71	NIST	Alkanones
Heptadecanone	C17H34O	254	43+**58**+71+254	NIST	
Alkanone	Unknown	x	43+**58**+71	NIST	
2-Pentanone	C5H10O	86	**43**+86	NIST	
Other aliphatics					
2-Pentene, 2,4-dimethyl-	C7H14	98	41+**55**+83+98	NIST	Other aliphatics
Nonanal	C9H18O	142	29+43+43+56+**57**+70+98	NIST	
Phenols					
Phenol	C6H6O	94	39+65+66+**94**	NIST	Phenols
Phenol, 4-methyl-	C7H8O	108	77+79+107+108	NIST	
Phenol, -dimethyl-	C7H8O	122	77+91+**107**+121+ **122**	NIST	
S compounds					
2(3H)-Benzothiazolone	C7H5NOS	151	96+123+**151**	NIST	S compounds
Benzenesulfonamide, N-butyl-	C10H15NO2S	213	51+**77**+141+170	NIST	
Steroids					
Stigmasta-3,5-dien-7-one	C29H46O	411	161+**174**+187+395+**410**	NIST	Steroids
(Poly)aromatics					
Toluene	C7H8	92	**91**+92	NIST	Toluene
Benzoic acid	C7H6O2	122	51+77+**105**+122	NIST	Benzoic acid
Naphthalene, 2-phenyl-	C16H12	204	101+**204**	NIST	Polyaromatics
Phenanthrene, 3,6-dimethyl-	C16H14	206	102+191+**206**	NIST	
Retene or Phenanthrene, 3,4,5,6-tetramethyl-	Both C18H18	234	165+178+**204+219+234**	NIST	
1,4-Diphenyl-1,3-butadiene	C16H14	206	91+128+191+**206**	NIST	(Alkyl)benzenes
Alkyl-Benzene C12	C18H30	246	**91+92**+…246	NIST	
Alkyl-Benzene C16	C22H38	302	**91+92**+…302	NIST	
Alkyl-Benzene C17	C23H40	316	**91+92**+…316	NIST	
Alkyl-Benzene C18	C24H42	330	**91+92**+…330	NIST	
Alkyl-Benzene C22	C28H50	386	**91+92**+…386	NIST	

[1] Chen et al., (2009) *Journal of Food Science*, 74: 100-105; [2] Fabbri et al., (2012) *Journal of Analytical and Applied Pyrolysis*, 95: 145-155

S5: Variability of elemental concentrations in digested aerosol filters, cloud water and precipitation

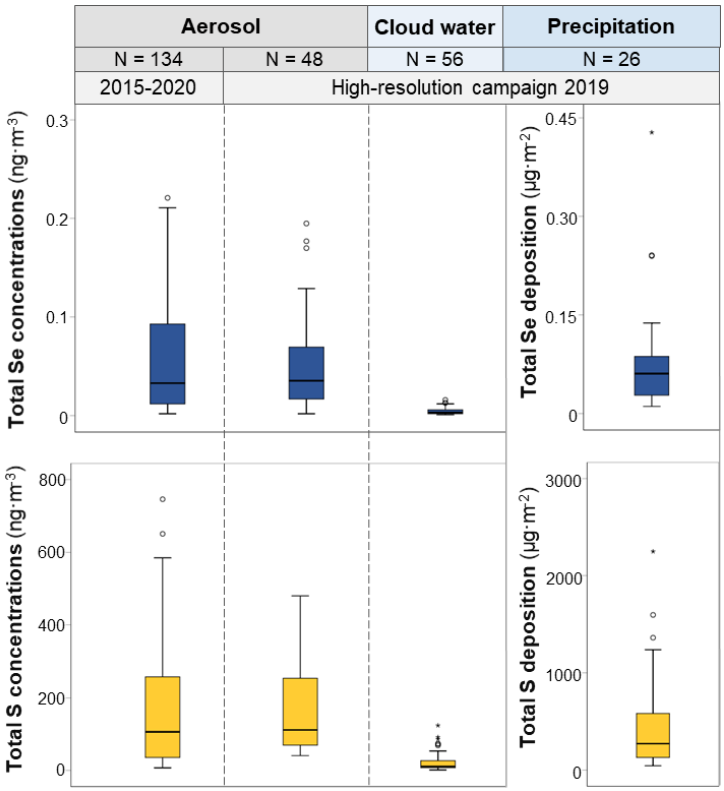

Fig. S4. Concentrations of total Se (shown in blue) and total sulfur (S; shown in yellow) in samples of digested aerosol filters collected during the 2015-2020 aerosol time series, as well as in aerosol filter digests, cloud water and precipitation (total deposition) samples collected during the campaign in 2019. Sample size of each sample type set is indicated with N.

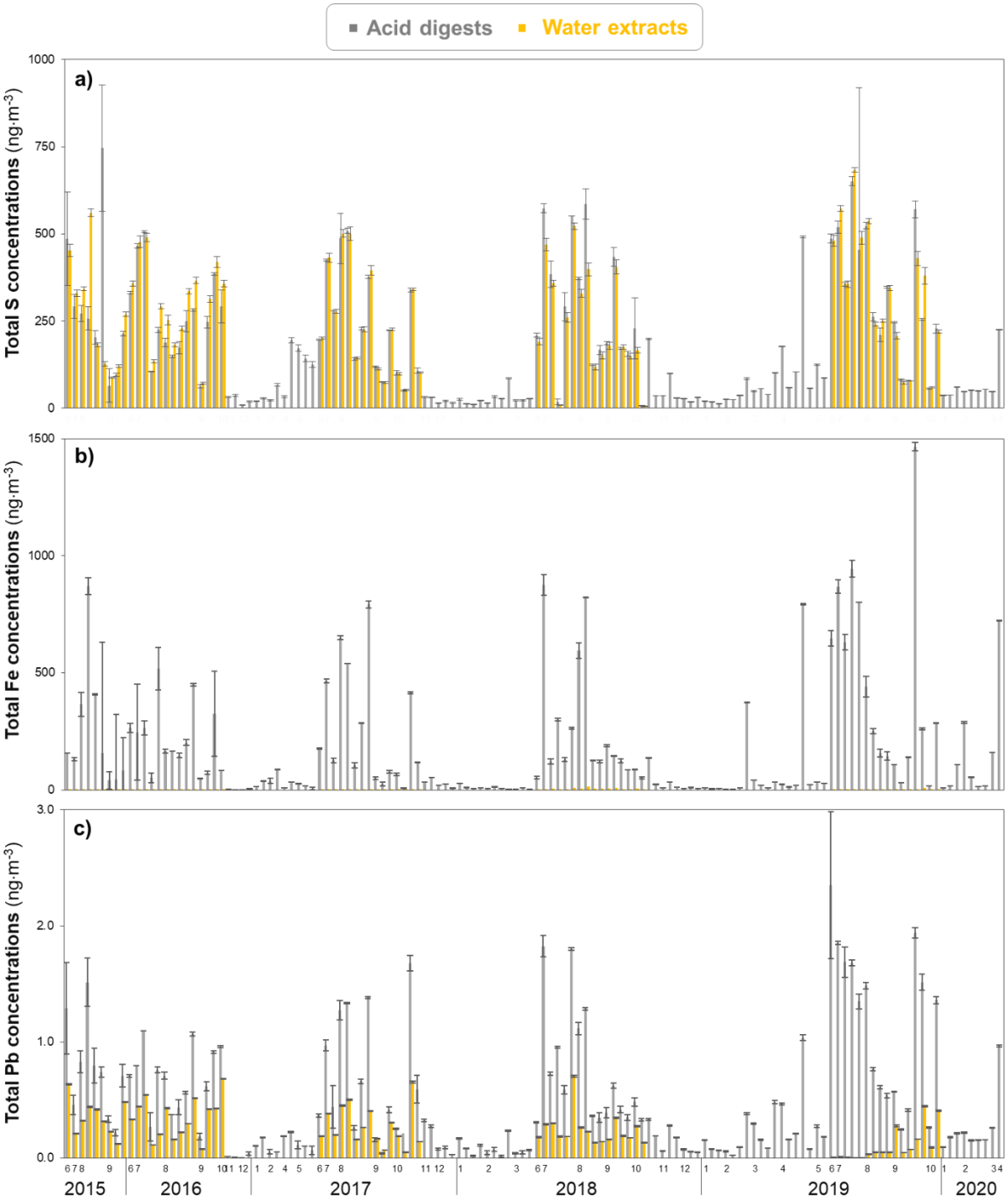

Fig. S5. Total concentrations of sulfur (S; panel a), iron (Fe; panel b) and lead (Pb; panel c) in acid digests (grey) and water extracts (yellow) of the aerosol filter from the 2015-2020 aerosol time series. The error bars represent the standard deviation values resulting from element quantification by ICP-MS/MS in triplicate.

S6: Source contribution of Se in aerosols by comparison between aerosol filter digest measurements and modelled Se concentration by SOCOL-AERv2

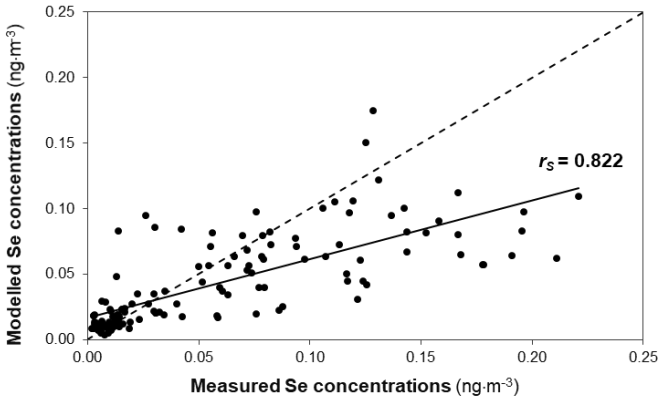

Fig. S6. Relationship between the Se concentrations in aerosol filter digests from the 2015-2020 aerosol time series obtained with the SOCOL-AERv2 model and those measured in acid digests by ICP-MS/MS analysis. The Se concentration values are shown as filled circles, the overall regression of values as a continuous line (correlation coefficient Spearman, r_S=0.822; p<0.01), and the 1:1 line (y=x) as a dashed line.

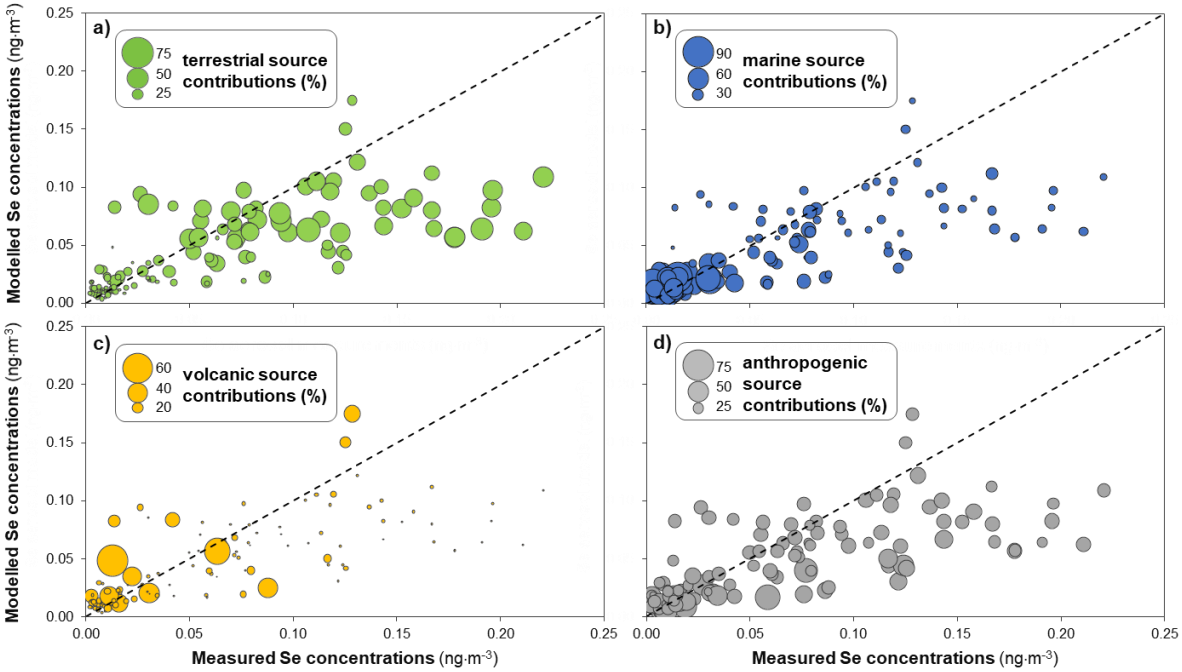

Fig. S7. Relationship between the Se concentrations in aerosol filter digests from the 2015-2020 aerosol time series obtained with the SOCOL-AERv2 model and those measured in acid digests by ICP-MS/MS analysis organized according to Se source contributions: a) terrestrial, b) marine, c) volcanic, and d) anthropogenic. The size of the data points correspond to proportions of respective modelled source contributions (in % total sources). The 1:1 line (y=x) is shown as a dashed line.

S7: Variability of moistures sources and water isotopes in precipitation and cloud water

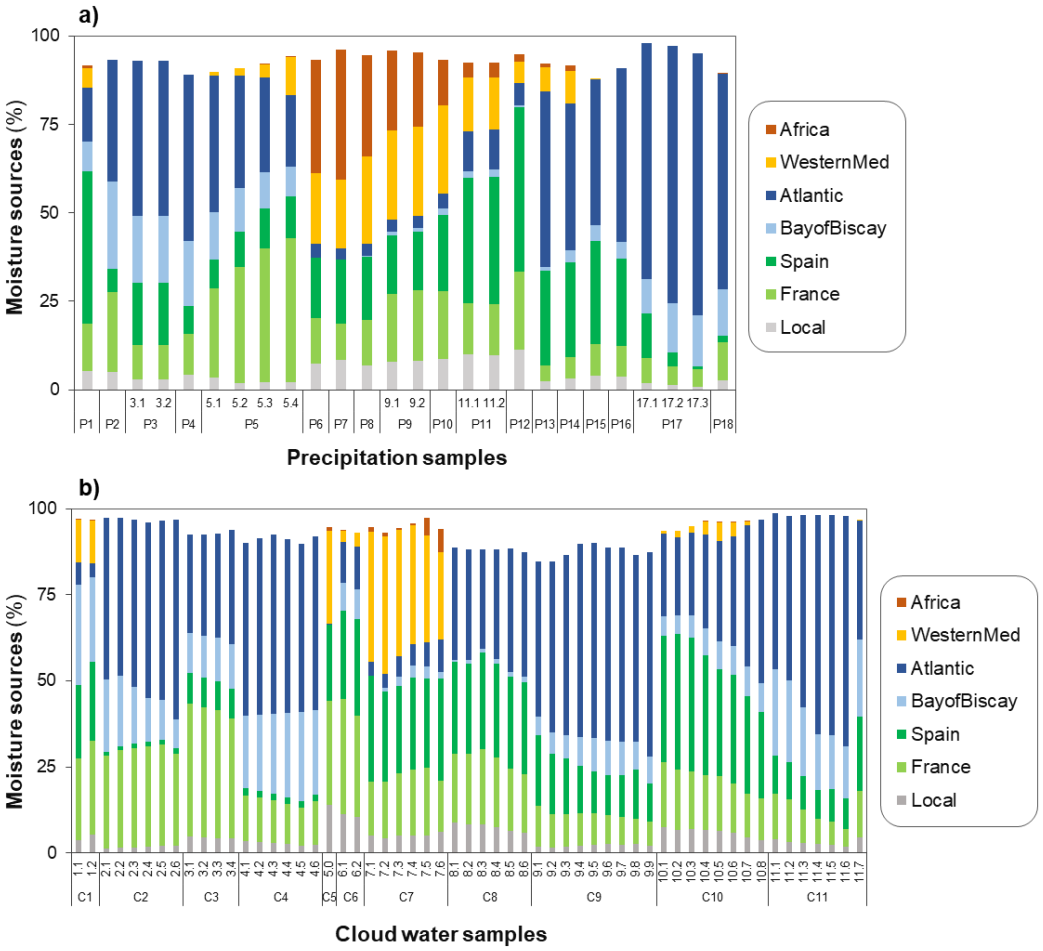

Fig. S8. Distribution of contributing moistures source of precipitation samples (panel a) and cloud water samples (panel b) collected during the campaign in 2019. In panel a, the x axis shows the 18 collected precipitation events (P1-P18), as well as their sub-samples for events P3, P5, P9, P11, and P17. In panel b, the x axis shows the 11 collected cloud events (C1-C11), as well as their sub-samples (for all events, except for event C5 for which only one sub-sample was taken). The data are shown as proportion of total moistures sources (%). Modelled regional moistures sources discussed in the manuscript include sources from France, Spain and Local. Modelled moistures sources with average values <3 % are not shown (e.g., moisture sources from Eastern Europe, America, Atlantic Subtropics, Portugal, UK, Ireland).

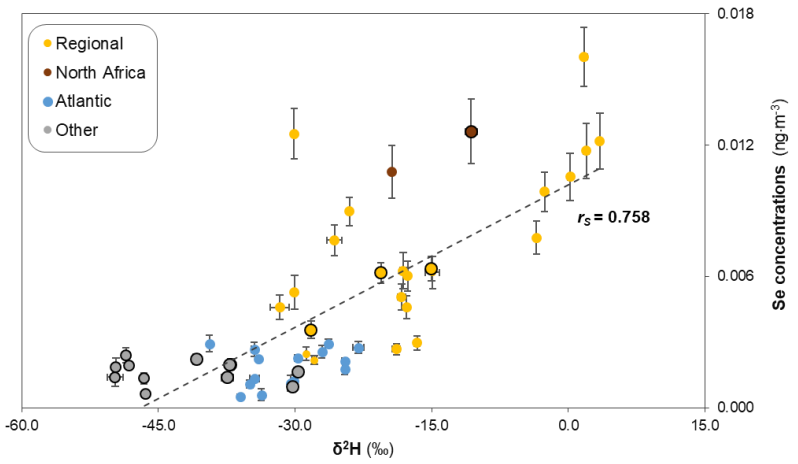

Fig. S9. Total Se concentrations and isotopic composition of deuterium (δ^2H: isotopic ratio relative to Vienna Standard Mean Ocean Water, expressed in per mill) in cloud water samples collected during the campaign in 2019. Each data point is coloured according to the dominant moisture sources of the cloud water samples, i.e., samples with dominant regional moisture sources (including moisture sources from France, Spain and Local) are shown in yellow, those with dominant moisture source from North Africa in brown, those with dominant moisture source from the Atlantic Ocean in blue, and those with dominant moisture source from other areas in grey. Sub-samples potentially influenced by precipitation are highlighted by a black symbol outline. Regional moistures sources discussed in the manuscript include sources from France, Spain and Local (local source, in France south of 43.6°N). The overall regression of values as a continuous line (correlation coefficient Spearman, r_S=0.758; p<0.01). The error bars for the y variable, i.e. Se concentration, represent the standard deviation values resulting from element quantification by ICP-MS/MS in triplicate. The error bars for the x variable, i.e. δ^2H, represent the standard deviation values resulting from stable water isotope analysis by Picarro in triplicate.

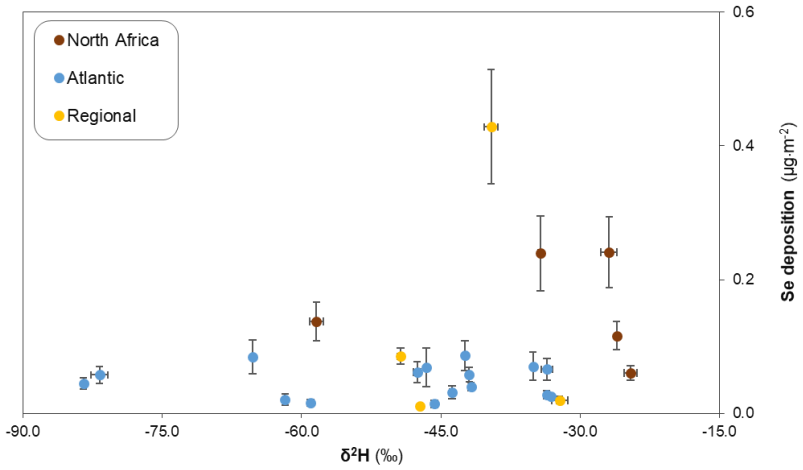

Fig. S10. Total selenium (Se) deposition and isotopic composition of deuterium (δ^2H: isotopic ratio relative to Vienna Standard Mean Ocean Water, expressed in per mill) in precipitation samples collected during the campaign in 2019. Each data point is coloured according to the dominant moisture sources of the precipitation samples, i.e., samples with dominant regional moisture sources (including moisture sources from France, Spain and Local) are shown in yellow, those with dominant moisture source from North Africa in brown, and those with dominant moisture source from the Atlantic Ocean in blue. Regional moistures sources include sources from France, Spain and Local (local source, in France south of 43.6°N). The error bars for the y variable, i.e. Se concentration, represent the standard deviation values resulting from element quantification by ICP-MS/MS in triplicate. The error bars for the x variable, i.e. δ^2H, represent the standard deviation values resulting from stable water isotope analysis by Picarro in triplicate.

Table S8. Additional information on sampled precipitation (sub-)events. The precipitation types include rain (RW), hail (H), snow/sleet (S/S), and light rain/cloud water (LR/CW).

Date	**Sub-event label**	**Sub-sampling time**	**Duration** (min)	**Precipitation type**	**Amount** (mL)	**pH**	**Rain rate** ($mm \cdot h^{-1}$)
01.09.2019	P1	04:15:00-5:15	60	LR/CW	190		0.4
05.09.2019	P2	03:45 – 10:00	375	LR/CW	264		0.1
10.09.2019	P3.1	02:10 - 09:10	420	S/S	1000	5.6	0.3
	P3.2	02:10 - 09:10	420	S/S	1000		0.3
10.09.2019	P4	09:30 – 11:45	135	S/S	450	5.6	0.4
10.09.2019	P5.1	17:45 – 20:00	135	S/S	759	5.5	0.7
	P5.2	20:00 – 21:00	60	S/S	653	5.6	1.4
	P5.3	21:00 – 22:30	90	S/S	555	5.6	1.2
	P5.4	22:30 – 01:30	180	S/S	391	5.6	0.4
14.09.2019	P6	19:20 – 19:50	30	RW	348		1.5
15.09.2019	P7	17:30 – 18:20	50	RW/H	1700	6.5	4.3
16.09.2019	P8	21:25-22:15	50	RW	1196	6.3	4.5
17.09.2019	P9.1	15:08-15:58	50	RW	657	7.2	1.7
	P9.2	15:58-16:08	10	RW/H	472	7.2	
18.09.2019	P10	17:00-8:00	900	RW	2108	6.8	2.2
18.09.2019	P11.1	15:14-16:10	56	RW/H	3101	6.0	9.5
	P11.2	15:14-16:10	71	RW/H	1138	6.0	9.5
19.09.2019	P12	22:00-24:00	120	RW	110		0.1
22.09.2019	P13	6:05-11:50	345	LR/CW	418	5.8	0.2
22.09.2019	P14	11:15-15:15	240	LR/CW	280	5.7	0.2
01.10.2019	P15	16:00-17:46	106	RW/H	1004	5.7	1.2
01.10.2019	P16	18:38-18:50	12	RW/H	973	5.4	10.2
02.10.2019	P17.1	1:00-5:30	270	S/S	960	5.4	0.5
	P17.2	5:30-11:50	380	S/S	2730	5.5	0.9
	P17.3	11:50-13:40	110	LR/CW	752	5.7	0.9
02.10.2019	P18	13:40-20:00	500	LR/CW	624	5.7	0.2

S8: High Se and other elements deposition associated with deep convective activity during thunderstorms

S8.1 Principle component analysis of precipitation samples

Variability in elemental concentrations in precipitation (given in $\mu g \cdot L^{-1}$) were explored using principal component analysis (PCA). The first two principal components (PC1-2) are shown in Fig. S11a. The precipitation volume was included passively in the PC-loading plots by using bivariate correlation coefficients between these variables and the PC scores of each PC. PC1 shows positive loadings of many major and trace elements (e.g. Na, K, P, Fe, Cu, Zn, As, Pb), which significantly correlate with the collected precipitation amount (p<0.05). Elemental concentration in precipitation are expected to be influenced by the dilution effect, which describes lower occurring concentrations at increasing rain volumes. PC scores of sub-events classified by their precipitation type, including events with rainwater/hail, light rain/cloud water or snow/sleet, show clear groupings on PC1 and PC2 (Fig. S11b). Particularly events that included light rain (light rain/cloud water) plot on PC1, which indicates that these events were primarily affected by the dilution effect.

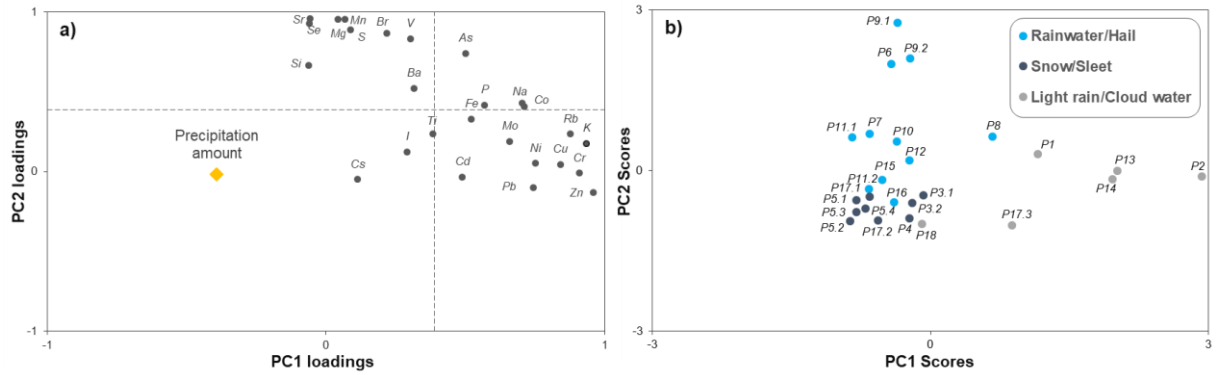

Fig. S11. Loading plot (panel a) and score plot (panel b) for principal components (PCs) 1–2 resulting from the principal component analysis performed with the element concentrations in precipitation samples from the 2019 campaign. PC1-2 account together for 63% of the total variance. For the PC-loadings, filled circles correspond to active variables, and the precipitation amount (yellow diamond) was added passively. Significance levels (PC-loading values >0.39) are indicated in loading plots by horizontal and vertical dashed line.

S8.2 Precipitation chemistry

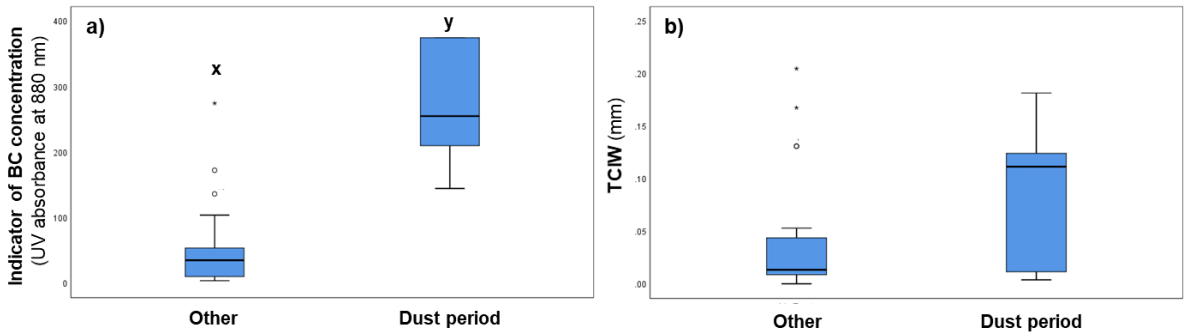

Fig. S12. Comparison between black carbon (BC; panel a) concentration (indicated by optical absorbing suspended particles at 880 nm) and the total column ice cloud water content (TCIW, in mm; panel b) during the dust period and all other events. The letters x and y denote that the two sample set are significantly different (Mann-Whitney-U test; $p<0.01$).

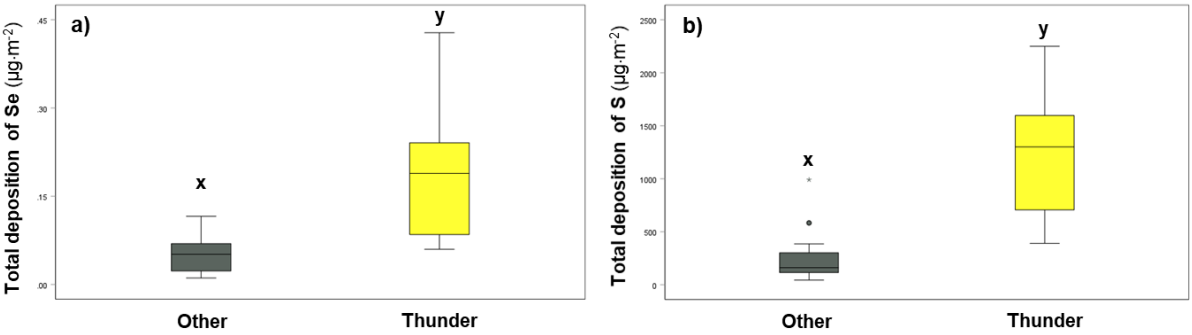

Fig. S13. Comparison between the total Se and S deposition during thunderstorms (yellow) and all other precipitation events (grey). Panel a) shows the data for Se and panel b) shows the data for S. The letters x and y denote that the two sample sets are significantly different in terms of total Se deposition in panel a and total S deposition in panel b (Mann-Whitney-U test; $p<0.01$).

S8.3 Aerosol chemistry and meteorological characteristics

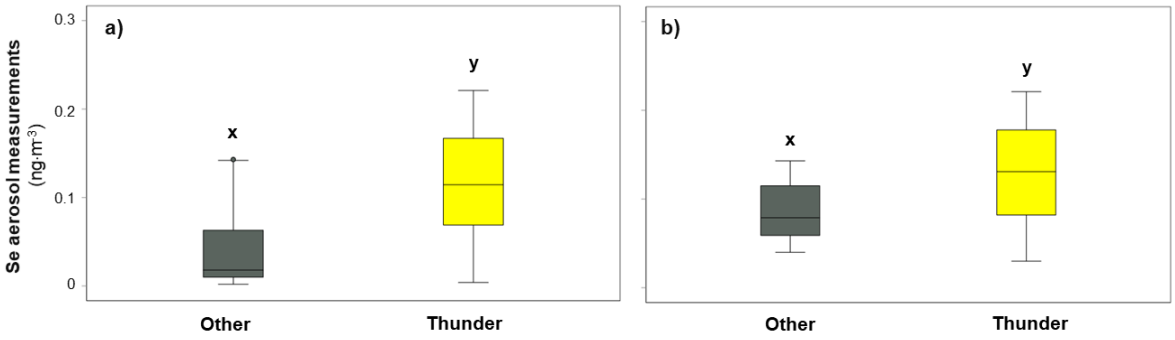

Fig. S14. Comparison between the total Se concentrations in aerosol filter digests from the 2015-2020 time series which were associated with (yellow) and without (grey) thunderstorms. Panel a) shows the Se concentrations in aerosol filter digests considering the entire 2015-2020 aerosol time series dataset. Panel b) shows the Se concentrations in aerosol filter digests considering only the samples taken during summer months. The letters x and y denote that the two sample sets are significantly different (Mann-Whitney-U test; $p<0.01$).

Table S9. *p* values associated to Mann-Whitney-U significant difference test performed between total concentrations of various elements in aerosol filter digests from the 2015-2020 aerosol time series associated with or not associated with thunderstorms when i) considering the entire 2015-2020 aerosol time series dataset (p values given in row "full series"); and ii) considering only the samples taken during summer months (*p* values given in row "only summer"). *p* values <0.01 are highlighted in green, while *p* values $p<0.05$ are highlighted in yellow. Elements with substantial periods of missing data were excluded from statistical analysis (i.e., Na, Ag, Cd and Ba).

	Se	As	S	Mg	Al	K	Ti	V	Cr	Mn	Fe	Co	Ni	Cu	Zn	Rb	Sr	Nb	Mo	Cs	Pb	U
full series	0.000	0.000	0.000	0.000	0.000	0.000	0.008	0.000	0.000	0.000	0.000	0.000	0.000	0.000	0.016	0.000	0.000	0.000	0.167	0.000	0.000	0.000
only summer	0.003	0.001	0.011	0.007	0.000	0.004	0.232	0.005	0.009	0.001	0.004	0.001	0.063	0.029	0.818	0.001	0.006	0.033	0.388	0.006	0.003	0.002

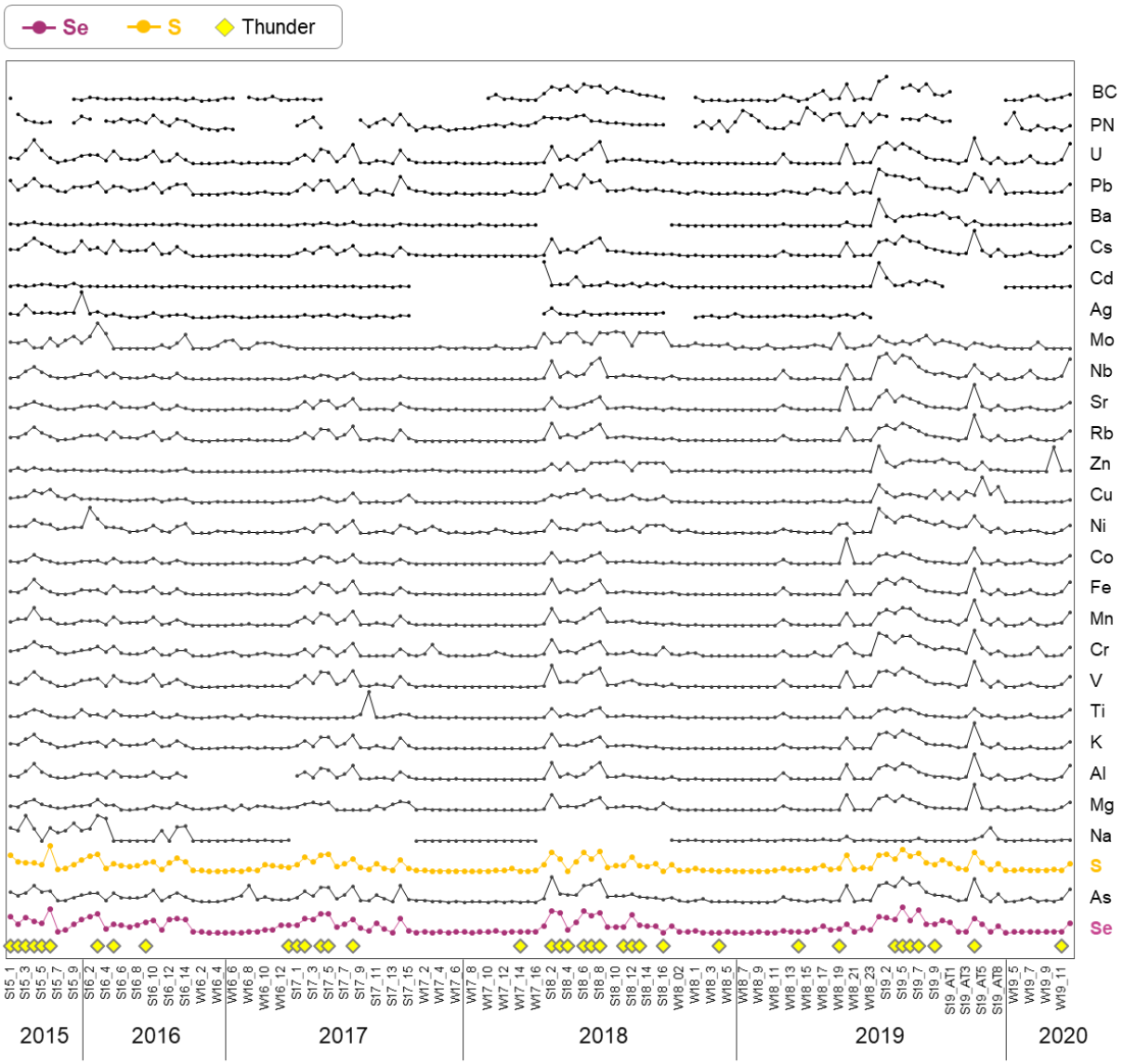

Fig. S15. Concentrations of measured elements in aerosol filter digests of the 2015-2020 aerosol time series. Additional chemical parameters shown include black carbon (BC) and particle number (PN). Aerosol samples associated with thunderstorms are shown at the bottom of the diagram with yellow diamonds.

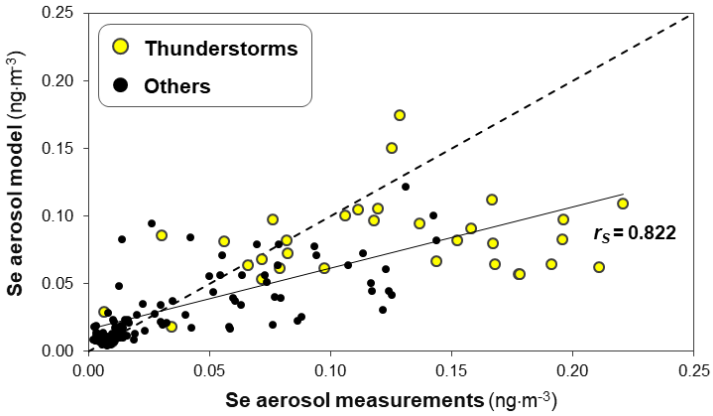

Fig. S16. Comparison of modelled SOCOL-AERv2 results with measurements of 2015-2020 aerosol time series. Se measurements in aerosol filter digests sampled during weeks with thunderstorms (shown as yellow circles, based on reported lightning activity by Blitzortung network within 3 km of Pic du Midi Observatory). All other aerosol measurements without detected thunderstorms during sampling are shown as black filled circles ("others"). The overall regression of all values is shown as a continuous line and the 1:1 line as a dashed line.

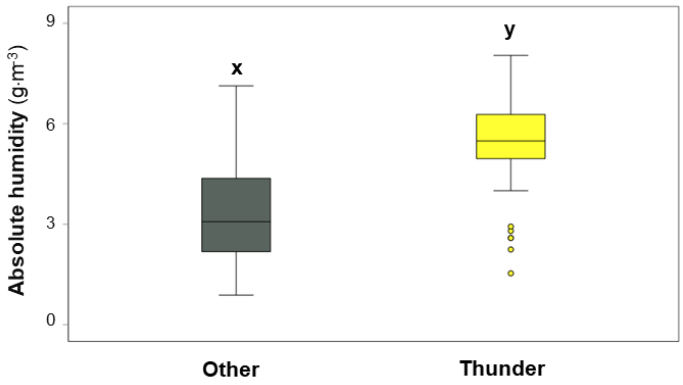

Fig. S17. Comparison between the absolute humidity for sampling periods in the 2015-2020 aerosol time series which were associated with (yellow) and without (grey) thunderstorms. Absolute humidity was calculated as (RH×Ps)/(Rw×T×100, with relative humidity (RH; %), Saturation vapour pressure (Ps; Pa), the specific gas constant for water vapour (Rw; 461.5 $J \cdot kg^{-1} \cdot K^{-1}$) and the air temperature (T, K). The letters x and y denote that the two sample sets are significantly different (Mann-Whitney-U test; $p<0.01$).

S9: Additional information on inorganic and organic Se and S speciation

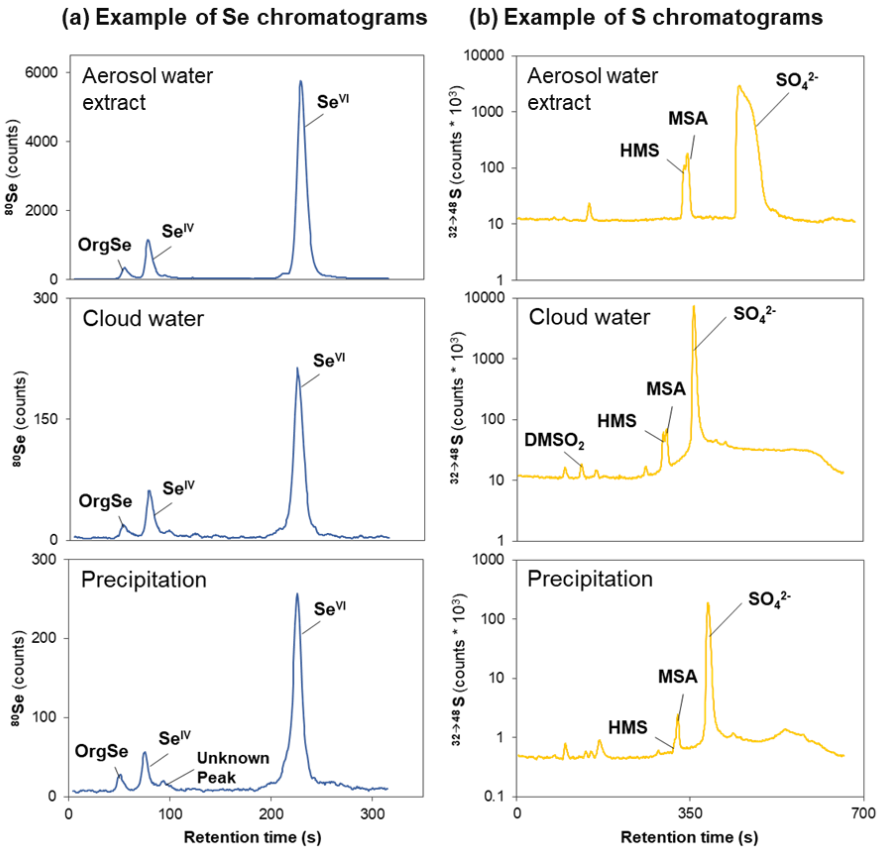

Fig. S18. Examples of intensity chromatograms of Se (panel a) and S (panel b) obtained for Pic du Midi aerosol water extracts (Se: S18_2, S: S18_12), cloud water (Se: C1.2, S: C12.1) and precipitation (Se: P8, S: P11.2). Identified Se and S species are indicated in respective chromatograms.

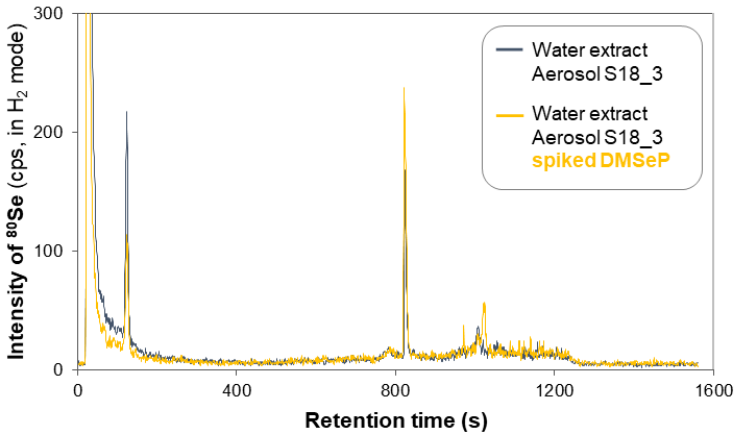

Fig. S19. Intensity chromatograms of Se in an aerosol water extract (unspiked; black line) and spiked with a dimethylselenonium propionate (DMSeP) standard (yellow line). These chromatograms were obtained, using an Ionosphere-5C column (Chrompack, 100x3 mm, 5 µm) and the procedure of Larsen et al. (2001), for the aerosol water extract S16_S3 from the 2015-2020 aerosol time series. DMSeP was spiked at 70 ng·L^{-1} using a DMSeP standard synthesized in-house according to published procedure by W.-M. Fan et al. (1998).

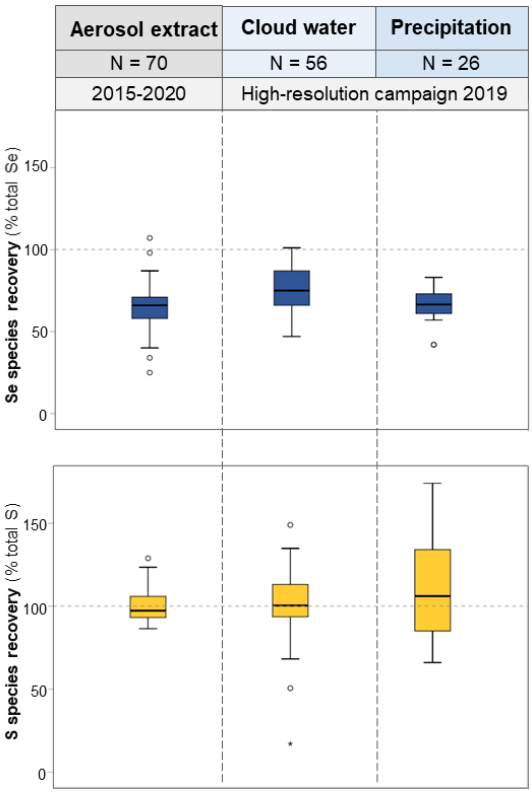

Fig. S20. Recoveries of Se (blue boxplots) and S (yellow boxplots) species in water extracts of aerosols from the 2015-2020 aerosol time series, as well as in cloud water and precipitation samples collected during the campaign in 2019. Recoveries of Se and S species are given in percentage of total Se and S concentrations in the samples, respectively. Recoveries of S above 100% are likely related to high and variable blank values for sulfate (SO_4^{2-}) leading to overestimation of SO_4^{2-} in samples with low S concentration. Sample size of each sample type set is indicated with N.

S10: Additional information on factors driving the deposited chemical form of Se

Table S10. Correlation coefficients between the abundance of (sub-)groups of organic compounds identified by Py-GC-MS and the proportions of Se species (with respect to total Se concentrations) for the 2015-2020 aerosol time series. Positive and negative correlations (determined using Spearman correlation coefficient) are highlighted in blue and orange, respectively. Different significance levels are indicated by colour strength: $^{**}p<0.01$ (dark blue/orange), $^{*}p<0.05$ (light blue/orange).

	Toluene	(Poly)-aromatics	Alkan-ones	Carbo-hydrates	Carboxylic acids	N-comp.	Alkanes	Alkenes	Other aliphatics	Phenols	S-comp.	Steroids	Protein	Levo-glucosan
Total Se	0.157	-0.121	-0.152	-0.230	0.141	-0.053	0.211	0.184	-0.149	0.099	**-0.314***	-0.015	0.130	**0.255***
Total water-soluble Se	0.169	-0.056	-0.180	-0.090	0.062	-0.017	0.190	0.235	-0.104	0.171	**-0.349****	0.031	0.198	0.243
OrgSe	**-0.474****	**-0.377****	-0.089	-0.046	0.192	**0.299***	-0.204	-0.106	0.086	-0.063	-0.160	**0.282***	**0.532****	0.149
Se^{IV}	**0.312***	**0.434****	-0.023	-0.209	-0.187	0.025	-0.011	-0.074	**-0.292***	0.085	**0.353****	-0.079	**-0.306***	**-0.354****
Se^{VI}	-0.098	-0.196	**0.296***	-0.178	-0.208	-0.068	0.184	**0.265***	0.246	**0.334****	-0.017	**-0.258***	-0.037	-0.108

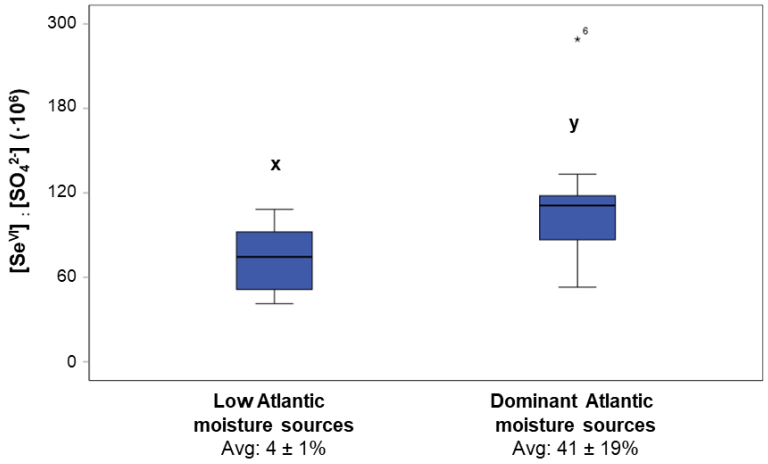

Fig. S21. Ratio between selenate (Se^{VI}) and sulfate (SO_4^{2-}) for precipitation events collected during the campaign in 2019 with low and dominant Atlantic moisture sources. The average contributions of Atlantic moisture sources of the two shown classifications are 4 ± 1% (low) and 41 ± 19% (dominant). The letters x and y denote that the two sample set are significantly different (Mann-Whitney-U test; $p<0.01$).

Supplementary References

Darrouzès, J., Bueno, M., Simon, S., Pannier, F., and Potin-Gautier, M.: Advantages of hydride generation interface for selenium speciation in waters by high performance liquid chromatography–inductively coupled plasma mass spectrometry coupling, Talanta, 75, 362-368, https://doi.org/10.1016/j.talanta.2007.11.020, 2008.

Gómez-Ariza, J. L., Pozas, J. A., Giráldez, I., and Morales, E.: Stability and Storage Problems in Selenium Speciation from Environmental Samples, International Journal of Environmental Analytical Chemistry, 74, 215-231, 10.1080/03067319908031427, 1999.

Larsen, E. H. and Stürup, S.: Carbon-enhanced inductively coupled plasma mass spectrometric detection of arsenic and selenium and its application to arsenic speciation, Journal of Analytical Atomic Spectrometry, 9, 1099-1105, 10.1039/JA9940901099, 1994.

Larsen, E. H., Hansen, M., Fan, T., and Vahl, M.: Speciation of selenoamino acids, selenonium ions and inorganic selenium by ion exchange HPLC with mass spectrometric detection and its application to yeast and algae, Journal of Analytical Atomic Spectrometry, 16, 1403-1408, 10.1039/B106355N, 2001.

Müller, E., von Gunten, U., Bouchet, S., Droz, B., and Winkel, L. H. E.: Hypobromous Acid as an Unaccounted Sink for Marine Dimethyl Sulfide?, Environmental Science & Technology, 53, 13146-13157, 10.1021/acs.est.9b04310, 2019.

Roulier, M., Bueno, M., Coppin, F., Nicolas, M., Thiry, Y., Rigal, F., Le Hécho, I., and Pannier, F.: Atmospheric iodine, selenium and caesium depositions in France: I. Spatial and seasonal variations, Chemosphere, 273, 128971, https://doi.org/10.1016/j.chemosphere.2020.128971, 2021.

Suess, E., Aemisegger, F., Sonke, J. E., Sprenger, M., Wernli, H., and Winkel, L. H. E.: Marine versus Continental Sources of Iodine and Selenium in Rainfall at Two European High-Altitude Locations, Environmental Science & Technology, 53, 1905-1917, 10.1021/acs.est.8b05533, 2019.

Tolu, J., Gerber, L., Boily, J.-F., and Bindler, R.: High-throughput characterization of sediment organic matter by pyrolysis–gas chromatography/mass spectrometry and multivariate curve resolution: A promising analytical tool in (paleo)limnology, Analytica Chimica Acta, 880, 93-102, https://doi.org/10.1016/j.aca.2015.03.043, 2015.

Tolu, J., Le Hécho, I., Bueno, M., Thiry, Y., and Potin-Gautier, M.: Selenium speciation analysis at trace level in soils, Analytica Chimica Acta, 684, 126-133, https://doi.org/10.1016/j.aca.2010.10.044, 2011.

W.-M. Fan, T., N. Lane, A., Martens, D., and M. Higashi, R.: Synthesis and structure characterization of selenium metabolites†, Analyst, 123, 875-884, 10.1039/A707597I, 1998.